

NASA/TM—2017-219480



Highly Conductive Wire: Cu Carbon Nanotube Composite Ampacity and Metallic CNT Buckypaper Conductivity

Henry C. de Groh III
Glenn Research Center, Cleveland, Ohio

April 2017

NASA STI Program . . . in Profile

Since its founding, NASA has been dedicated to the advancement of aeronautics and space science. The NASA Scientific and Technical Information (STI) Program plays a key part in helping NASA maintain this important role.

The NASA STI Program operates under the auspices of the Agency Chief Information Officer. It collects, organizes, provides for archiving, and disseminates NASA's STI. The NASA STI Program provides access to the NASA Technical Report Server—Registered (NTRS Reg) and NASA Technical Report Server—Public (NTRS) thus providing one of the largest collections of aeronautical and space science STI in the world. Results are published in both non-NASA channels and by NASA in the NASA STI Report Series, which includes the following report types:

- **TECHNICAL PUBLICATION.** Reports of completed research or a major significant phase of research that present the results of NASA programs and include extensive data or theoretical analysis. Includes compilations of significant scientific and technical data and information deemed to be of continuing reference value. NASA counter-part of peer-reviewed formal professional papers, but has less stringent limitations on manuscript length and extent of graphic presentations.
- **TECHNICAL MEMORANDUM.** Scientific and technical findings that are preliminary or of specialized interest, e.g., “quick-release” reports, working papers, and bibliographies that contain minimal annotation. Does not contain extensive analysis.
- **CONTRACTOR REPORT.** Scientific and technical findings by NASA-sponsored contractors and grantees.
- **CONFERENCE PUBLICATION.** Collected papers from scientific and technical conferences, symposia, seminars, or other meetings sponsored or co-sponsored by NASA.
- **SPECIAL PUBLICATION.** Scientific, technical, or historical information from NASA programs, projects, and missions, often concerned with subjects having substantial public interest.
- **TECHNICAL TRANSLATION.** English-language translations of foreign scientific and technical material pertinent to NASA's mission.

For more information about the NASA STI program, see the following:

- Access the NASA STI program home page at <http://www.sti.nasa.gov>
- E-mail your question to help@sti.nasa.gov
- Fax your question to the NASA STI Information Desk at 757-864-6500
- Telephone the NASA STI Information Desk at 757-864-9658
- Write to:
NASA STI Program
Mail Stop 148
NASA Langley Research Center
Hampton, VA 23681-2199



Highly Conductive Wire: Cu Carbon Nanotube Composite Ampacity and Metallic CNT Buckypaper Conductivity

Henry C. de Groh III
Glenn Research Center, Cleveland, Ohio

National Aeronautics and
Space Administration

Glenn Research Center
Cleveland, Ohio 44135

Acknowledgments

Thanks are due Diana Santiago for her help and tutoring throughout this work and in particular for her assistance with Raman spectroscopy. Similarly, many thanks are given to Daniel Scheiman for his help with the spectroscopy. A significant fraction of this paper is due to the generous collaboration of Kyle Kissell whose company provided the Cu-CNT composite wire.

This work was sponsored by the Advanced Air Vehicle Program
at the NASA Glenn Research Center

Level of Review: This material has been technically reviewed by technical management.

Available from

NASA STI Program
Mail Stop 148
NASA Langley Research Center
Hampton, VA 23681-2199

National Technical Information Service
5285 Port Royal Road
Springfield, VA 22161
703-605-6000

This report is available in electronic form at <http://www.sti.nasa.gov/> and <http://ntrs.nasa.gov/>

Highly Conductive Wire: Cu Carbon Nanotube Composite Ampacity and Metallic CNT Buckypaper Conductivity

Henry C. de Groh III
National Aeronautics and Space Administration
Glenn Research Center
Cleveland, Ohio 44135

Abstract

NASA is currently working on developing motors for hybrid electric propulsion applications in aviation. To make electric power more feasible in airplanes higher power to weight ratios are sought for electric motors. One facet to these efforts is to improve (increase) the conductivity and (lower) density of the magnet wire used in motors. Carbon nanotubes (CNT) and composites containing CNT are being explored as a possible way to increase wire conductivity and lower density. Presented here are measurements of the current carrying capacity (ampacity) of a composite made from CNT and copper. The ability of CNT to improve the conductivity of such composites is hindered by the presence of semiconductive CNT (s-CNT) that exist in CNT supplies naturally, and currently, unavoidably. To solve this problem, and avoid s-CNT, various preferential growth and sorting methods are being explored. A supply of sorted 95 percent metallic CNT (m-CNT) was acquired in the form of thick film Buckypaper (BP) as part of this work and characterized using Raman spectroscopy, resistivity, and density measurements. The ampacity (A/cm^2) of the Cu-5vol%CNT composite was 3.8 percent lower than the same gauge pure Cu wire similarly tested. The lower ampacity in the composite wire is believed to be due to the presence of s-CNT in the composite and the relatively low (proper) level of longitudinal cooling employed in the test method. Although Raman spectroscopy can be used to characterize CNT, a strong relation between the ratios of the primary peaks G/G' and the relative amounts of m-CNT and s-CNT was not observed. The average effective conductivity of the CNT in the sorted, 95 percent m-CNT BP was 2.5 times higher than the CNT in the similar but un-sorted BP. This is an indication that improvements in the conductivity of CNT composites can be made by the use of sorted, highly conductive m-CNT.

Scope and Background

Conductive wire has very wide applications throughout the world economy. Applications of interest to NASA are primarily for power cables and what is known as “magnet wire” (Ref. 1). The term magnet wire refers to the magnetic field created by the wire when it is wound into a coil and current is passed through it. These cables and wires are used throughout aircraft and spacecraft. NASA is currently developing hybrid electric power systems for aircraft such as those presented by Rolt and Whurr (Ref. 2) and Welstead and Felder (Ref. 3) in an effort to improve aviation efficiency and lower environmental impacts (Ref. 4). Improvements in the properties of wire are applicable to all kinds of technologies which include all electric motors, power transmission, hybrid automobiles, and current aviation and space technologies; improvements in wire conductivity and density are believed required for the advancement of hybrid electric power in aircraft.

Copper is usually used for magnet wire while Al is widely used for power transmission due to its low cost, and in airplanes due to its low density. In a motor, use of Al wire is usually not advantageous because the larger diameter (or greater number of turns) Al wire required to get equivalent power (due to its lower conductivity) negatively impacts other aspects of the motor. These two materials have the best combinations of cost, electrical conductivity, and density for applications of interest to NASA. The goals of this work are to improve the conductivity and density of magnet and transmission wire. To make these improvements additions of carbon nanotubes (CNT) to matrix materials Cu or Al are being explored.

A CNT can be thought of as being like a straw you might use to drink with. The material the straw is made of is a sheet of carbon in the case of the CNT. This sheet of carbon is known as graphene (Ref. 5); graphene is a sheet consisting of a hexagonal lattice of atomic, sp^2 carbon, one carbon atom thick. The structure of the CNT made from this sheet depends on how the atoms wrap around and combine. This structure and the effective twisting of the graphene lattice are described by chiral vectors and their translational coefficients n_1 and n_2 . The resulting properties of the CNT depend greatly on this structure, on the CNT's chirality (Ref. 5). It has been found that when $2(n_1) + n_2$ is a multiple of 3 the CNT is "metallic" (m-CNT) with characteristically high thermal and electrical conductivity; all other cases resulting in CNT with properties characteristic of semiconductors (s-CNT). The probabilities of possible combinations work out such that about 66 percent of the CNT are s-CNT, and ~33 percent are m-CNT. This is an extremely important reality currently. Processes are being developed to either sort or preferentially grow s-CNT or m-CNT, but at this time, unless proven otherwise, CNT supplies consist of a 66/33 mix of s-CNT/m-CNT (Refs. 5 and 6).

For many applications it is very inconvenient for the m-CNT and s-CNT to be mixed together. For semi-conductor applications, the m-CNT cause unwanted short circuits; and s-CNT cause low thermal and electrical properties in composites with Cu and Al. Thus there has been significant interest in both separation and selective growth techniques (Ref. 6). Kay Hyeok An et al. removed the m-CNT from the mix by destroying them in solution using nitronium ions; though the process was only effective for diameters less than 1.1 nm (Ref. 7). Zhang et al. similarly destroyed the m-CNT using a "dry" gas-phase plasma hydrocarbonation reaction to selectively etch and gasify the m-CNT (Ref. 8). Ding et al. employed single crystal quartz substrates and methanol to selectively grow s-CNT (Ref. 9) and Qu, Du, and Dai reported the preferential growth of semiconducting single-walled CNT (SWNT) by plasma-enhanced chemical vapor deposition (Ref. 10). Hong et al. directly grew s-CNT with the assistance of ultraviolet irradiation (Ref. 11). Harutyunyan and co-workers selectively enriched the growth of m-CNT through manipulation of the Fe nanocatalysts used to promote growth (Ref. 12). Others have developed sorting techniques which employ alternating current dielectricphoresis (Ref. 13), surface functionalities and device fabrication (Ref. 14), density differentiation (Ref. 15), and gel agarose chromatography (Ref. 16). Though there has been much work on efficiently selectively growing, and sorting CNT, sorted CNT are still not readily available, and when a supply can be found, quantities are very small, and prices very high (~\$60,000/g). Once growth and sorting technologies are better developed, and since carbon is one of the most abundant elements on Earth, it is hoped that the price for CNT will eventually be less than metals such as Cu and Al.

This work is a continuation of work previously published (Ref. 1); background material and references will not be repeated here, however a brief summary is provided below:

The conductivity of Cu, a CNT yarn, and a dilute Cu-CNT composite was measured at temperatures up to 340 °C. The conductivity of the Cu-CNT composite was about 3 percent lower than pure copper's at all temperatures. The conductivity of the CNT yarn was about 200 times lower than copper's, however, the yarn's conductivity dropped less with increasing temperature compared to Cu. The conductivity and density of CNT composites generally follow rule-of-mixtures, which is a weighted average based on volume fractions; thus any constituent that takes up cross sectional area will influence conductivity. Single-walled CNT have smaller cross sectional areas and the inner tubes in multi-walled CNT (MWNT) may not contribute to conduction. For these reasons single-walled CNT have an advantage over MWNT when high conductivity and low density are desired. To maximize CNT composite conductivity the volume fraction of m-CNT should be maximized. Other factors believed to strongly affect conductivity include interfacial resistances, matrix conductivity, and void fraction. Tests done on a Cu-CNT composite found the conductivity of m-CNT, including interfacial resistances present in this case, to be higher than copper's. This implies a Cu-CNT composite could be made with improved conductivity and density compared to copper (Ref. 1).

This memorandum presents recent results on:

- Ampacity measurements of the same dilute Cu-CNT composite (TerraCopper) presented in Reference 1.
- Raman Spectroscopy of powder and thick film Buckypapers made from a variety of CNT which include: MWNT; few-walled CNT (FWNT); mixed SWNT and sorted, metallic only SWNT (m-SWNT).
- Conductivity and density measurements of Buckypapers made from mixed and sorted SWNT.

Buckypaper (BP) is the paper resulting from removing (filtering) CNT from solution; it is a precursor state, to be further processed in later steps. For the development of wire BP might for example be dissolved and dispersed in solution and coated with Cu using electroless plating, then removed from solution to form BP again and perhaps consolidated into a Cu-CNT composite wire. Various processes in solution are needed to treat, purify, sort, or coat CNT. Buckypaper is the solid thick film formed by the CNT when the solution is removed. Buckypaper can be examined between these various steps yielding information about the CNT.

Xue measured the resistivity of SWNT BP from two vendors and found it to be about 7×10^{-3} for one, and 1.5×10^{-2} Ohm-cm for the other (Ref. 17). Buckypaper frequently has residual surfactants; surfactants such as Triton X-100 are used to aid dispersion and suspension in earlier processing steps. These surfactants can cause problems in later steps (such as inhibit interfacial bonding) thus usually need to be removed, or washed out of the BP. Xue found the resistivity of unwashed, and washed SWNT BP to be 2.1×10^{-2} and 6×10^{-3} Ohm-cm respectively (Ref. 17). Xue experimented with different solvents as surfactants including Triton X-100 and Chloroform, and measured the resulting BP resistivity after washing the solvents out; the resistivity of the Buckypapers made with Triton X-100 and Chloroform were 4.4×10^{-3} and 1.8×10^{-3} Ohm-cm, respectively (Ref. 17).

Raman spectroscopy can be used to observe vibrational, rotational, and other low-frequency modes in a material; it relies on inelastic scattering of laser light. The laser light interacts with molecular vibrations, phonons, or other excitations resulting in the energy of the laser phonons being shifted up or down. Raman spectroscopy is an established tool for the analysis of CNT (Ref. 18). The features of the Raman spectra considered in this study are the G and G'-bands, D-band, and the radial breathing modes (RBM). Carbon can exist in different forms, or hybridizations. Three of these forms are sp, sp², and sp³ which refer to their structures: sp is a linear chain of carbon atoms; in sp² each carbon atom is attached to three other carbon atoms with all atoms being in the same plane, forming a flat triangle; sp³ occurs when a carbon atom is bonded to 4 other carbon atoms, making a tetrahedral. The structure of diamond is sp³. Graphite, graphene, and CNT consist mainly of sp² structures. In carbon materials there is only one first-order Raman peak; this peak is referred to as the G-band. For sp² carbon the G-band peak appears near 1582 cm⁻¹, for diamond (sp³) the G-band peak appears near 1333 cm⁻¹, and in the range of 1850 to 2100 cm⁻¹ for sp. Thus for example, a strong Raman spectral peak seen near 1582 cm⁻¹ is an indication of the presence of sp² carbon. It should be noted that carbon materials exhibit "dispersive" behavior, which is a change in the phonon frequency (peak location) with laser excitation energy (Ref. 18). Through consideration of various peaks, Raman spectroscopy was used to characterize the quality and relative amounts of s-CNT and m-CNT in as-received supplies of various CNT (Refs. 18 and 19). Infrared spectroscopy is another valuable tool for quantifying the s-CNT/m-CNT mix of CNT supplies (Refs. 15 and 20) that shall be included in future work.

This work is limited to direct current (DC) resistance measurements and calculations only. Even though we expect applicable motors to use alternating current (AC) DC resistance values are appropriate because the expected AC frequency should be low enough to omit the need to consider any Skin Effect (Ref. 21) on conductivity. The AC frequency used in aviation motors is expected to be near 100 Hz and the skin depth for Cu wire at 100 Hz is about 7 mm, which is much greater than probable motor winding wire radii.

Experimental Procedures

This section presents: the procedures used to measure the current carrying capacity, frequently known as ampacity, of 20 AWG wires made from Cu, a dilute approximately Cu-5vol%CNT composite with the trade name TerraCopper, and a 28 AWG CNT yarn; Raman spectroscopy of CNT BP and powder; and the resistivity (and conductivity) and density of BP made from purified SWNT and sorted SWNT which were also purified.

Current Carrying Capacity (Ampacity)

In these experiments two samples of 20 AWG Cu magnet wire were compared to three samples of similar gauge TerraCopper Cu-CNT composite wire, and two samples of 28 AWG CNT yarn. The TerraCopper was supplied by NanoRidge Materials Inc.; in a previous study it was determined that the composite was dilute, with a fairly low volume fraction CNT (Ref. 1). The CNT yarn was supplied by Nanocomp Technologies Inc.; the makeup of this yarn in terms of number of walls and purity are unknown, though it is expected to contain MWNT. Each specimen was about 2.2 in. (5.59 cm) long.

Cross sectional area is an important part of the ampacity measurement since ampacity is the current at failure divided by the cross sectional area. The diameter of each wire specimen was measured eight times using calibrated calipers with each measurement taken at a different longitudinal, and azimuthal location. The average diameter was used to calculate cross sectional area.

Currents of the order of 100 A were expected in these tests, thus very heavy #2/0 AWG, 600 V, welding cable was used for lead cables from the HP 6011A DC Power Supply and test terminals. The wire specimens were clamped to custom-made Cu terminals made from 0.5 in. (1.27 cm) diameter Cu bar; the contact surfaces were sanded and cleaned prior to testing. Three Type-K thermocouples were connected to the wire; one in the center, and the other two located about 0.15 in. (0.38 cm) from each terminal. The inner distance between the terminals was approximately 1 in. (2.54 cm). The power supply was set to constant current mode, and the current raised very slowly from zero; voltage was also monitored. The current was manually raised a small amount and held at some specific value while the temperatures and voltage were monitored. After stabilization of temperature and voltage, the current was raised and held again. This was repeated, slowly raising current until failure due to runaway rising of temperature and melting of the wire. All wire failures were very near the center, midpoint between the terminals. Figure 1 is an image of part of the ampacity test systems, showing the cable connected to the terminals and the failed specimen.



Figure 1.—Ampacity measurement of 20 AWG wire; the Cu connecting rods are 0.5 in. diameter.

Raman Spectroscopy

A DXR Raman Microscope from Thermo Scientific was used to characterize and compare the following CNT from different suppliers:

- MWNT—Multi-wall CNT Buckypaper made from a natural mixture of m-CNT and s-CNT.
- FWNT—meaning few-walled CNT, this powder with the product designation of FW100X was supplied by Southwest NanoTechnologies, Norman Oklahoma (Ref. 22). FW100X is reported to be 93 to 97 wt% pure carbon, with median wall number of 2, median tube outer diameter of 2.45 nm, median tube length of 2.3 μm , and a Raman G to D-band peak ratio of 20 (using a 633 nm laser).

NanoIntegris Quebec Canada (with satellite offices in Skokie IL) supplied IsoNanotubes-M and Super PureTubes SWNT Buckypapers (Ref. 20):

- Mixed SWNT—Super PureTubes are advertised as being the same as IsoNanotubes-M, but have not been sorted, thus are expected to be a mixture of approximately 66 percent s-SWNT: 33 percent m-SWNT, this batch will be referred to as “mixed” or mixed-SWNT.
- Sorted SWNT—IsoNanotubes-M are said to be sorted SWNT such that 95 percent are metallic; material from this batch will be referred to as “sorted” or m-SWNT.

Both Super PureTubes and IsoNanotubes-M were made by arc discharge, have a mean diameter of 1.4 nm, mean length of 0.5 to 1 μm , 0.5 to 1 wt% catalyst impurity, and <5 percent carbonaceous impurity. According to NanoIntegris, IsoNanotube-M and Super PureTubes are the same except IsoNanotube-M are sorted, and have approximately 5 wt% residual iodine.

For all Raman spectroscopy the laser excitation wavelength was 633 nm, with the instrument set to full-range grating, 6 cm^{-1} spectral resolution, 3500 cm^{-1} upper cutoff, 50 cm^{-1} lower cutoff, and a spot size of 2.5 μm . Laser powers between 2 and 7 mW were explored. To determine the sensitivity of the results to laser power, tests were done of the same area using different power settings. To determine the sensitivity of the results to the specific location on a BP sheet and to the “top” or “bottom” side of the BP, tests were done at constant power on different areas and on the top and bottom sides of the BP. The resulting data was normalized (divided by) to the first-order G-band peak (near 1582 cm^{-1}) with repeat results for a given sample at the same laser power averaged.

The G-band peak is made up of G^+ and G^- peaks at ~ 1593 and ~ 1526 cm^{-1} , respectively. The G^- peak in metallic SWNT is uniquely strong, causing asymmetry, and a downshift, widening the G-band peak, resulting in a so called Breit-Wigner-Fano (BWF) line shape. Semiconducting tubes usually result in a G-band peak with a Lorentzian line shape. These characteristic shapes were considered as indications of the metallic or semiconductive nature of the samples. Use of the G-band shape to assess the electronic nature of SWNT may be problematic because intensity also depends on the chiral angle, particularly for SWNT with chiral angles resulting from zig-zag ($n_1, 0$) structures, which can be metallic or semiconducting (Refs. 5 and 19).

Low frequency radial breathing mode (RBM) peaks (near 100 to 500 cm^{-1}) are a strong unique feature in SWNT and FWNT, and provide direct evidence of the presence of single or double-walled versus multi-walled CNT. The RBM frequency, ω_{RBM} , is proportional to tube diameter, d_t , and has been found to be approximately

$$\omega_{\text{RBM}} = C/d_t \quad (1)$$

where $C = 248$ for an isolated CNT, with ω in cm^{-1} , and d_t in nm (Refs. 19 and 22). The RBM peaks were examined to estimate tube diameter. Radial breathing mode peaks can also be used to indicate the electronic nature of the SWNT, with peaks between 175 and 210 cm^{-1} being metallic; and peaks ranging from 130 to 160 cm^{-1} being due to semiconductive SWNT (Refs. 9 and 12).

The peak near 1350 cm^{-1} is called the disorder-induced D-band and is due to elastic scattering by defects, thus the ratio of G/D peaks was used to quantify CNT defect density.

The intensity of the G' band near 2600 cm^{-1} has a strong dependence on the metallicity of the sample (Ref. 19). The ratio of the G to G' bands was used as an indicator of the presence of m-CNT.

Buckypaper Resistivity

Two batches of SWNT BP were tested, both supplied by NanoIntegris of Quebec Canada (and Skokie IL). These materials are detailed in their technical data sheet (Ref. 20): IsoNanotubes-M are said to be sorted SWNT such that 95 percent have metallic properties, material of this batch will be referred to as “sorted” or m-SWNT; PureTubes are advertised as being the same as IsoNanotubes-M, but have not been sorted, thus are expected to be a mixture of approximately 66 percent s-SWNT: 33 percent m-SWNT, this batch will be referred to as “mixed”. Both batches were made by arc discharge, have a mean diameter of 1.4 nm, mean length of 0.5 to 1 μm , 0.5 to 1 wt% catalyst impurity, and <5 percent carbonaceous impurity. Figure 2 shows examples of the mixed and sorted BP. Small strips were cut from the central sections of the BP for conductivity measurements. Samples were taken from three different sheets of each batch. Strip samples as shown in Figure 2(b) were approximately 0.3 cm wide, 3 cm long, by 0.03 mm thick. The width and thickness were measured at four locations along the length of each strip and averaged to determine the cross sectional area, A , of each specimen. A calibrated Keithley 580 micro-ohmmeter was used to measure the resistance of each strip; the micro-ohmmeter was set up with two source, and two sensing flat jawed micro-clips. The contact surfaces of the clips were sanded and cleaned prior to testing. The resistance, R , and length between the sensing clips, L , was measured two or three

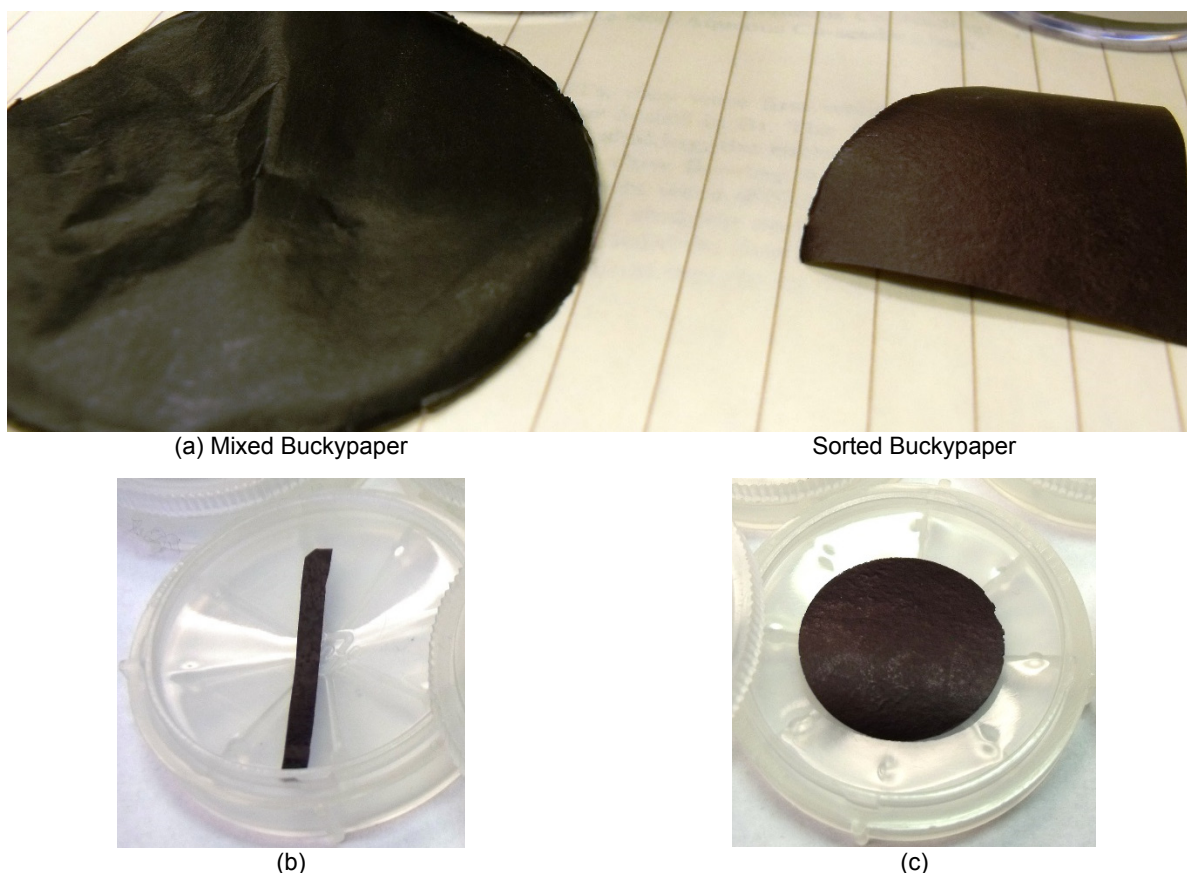


Figure 2.—(a) As-received sheets of mixed and sorted BP; (b) 0.3 cm wide strip for resistivity measurements; (c) 2.6 cm diameter disk cut for density measurements.

times for each strip, the average of which was used to calculate BP resistivity: $\rho_B = R \cdot A/L$. This is the resistivity of the BP, which is influenced by many things, including the conductivity of the CNT, contact resistance between the CNT, void fraction, and the presence of impurities and residual catalysts. In an effort to learn more about the relative conductivity of the CNT in the BP, void fraction was measured. Void fraction was determined by using rule-of-mixtures, BP density measurements, and an assumed CNT density, $D_{CNT} = 2 \text{ g/cm}^3$.

Buckypaper Density

One inch (2.6 cm diameter) disks similar to the one shown in Figure 2(c) were cut from two sheets of each batch for density measures. The thickness of each disk was measured four times, these were averaged. The mass of each disk was measured twice and averaged. These measurements enabled the calculation of BP density, D_B , and void fraction using the following rule-of-mixtures:

$$D_B = D_{CNT}(\phi_{CNT}) + D_{void}(\phi_{void}) \quad (2)$$

where ϕ is volume fraction and the density of the void space, D_{void} , is equal to zero, making the volume fraction of CNT in the BP

$$\phi_{CNT} = D_B / D_{CNT} = D_B / (2 \text{ g/cm}^3) \quad (3)$$

Results

Ampacity

The average ampacity of the wire specimens tested is presented in Figure 3. The variation of the Cu ampacity measurements was ± 1.6 percent, for TerraCu ± 2 percent, and ± 10 percent for the yarn. Contrary to other accounts (Ref. 23) and claims (Ref. 24) the CNT present in the TerraCu did not improve the material's ampacity. Likely reasons for the low ampacity in the TerraCu include the presence of s-CNT and the low volume fraction CNT employed in the composite. Ampacity is not a material property. It is a measurement that can be influenced by experimental factors such as levels of cooling. When a long wire is placed in service and is getting warm due to current flow it must shed that heat out radially- not longitudinally. In the ampacity testing of very expensive CNT composite wire it is common practice to use a rather short section of wire, connected at its ends to very heavy connectors; it is also common to imbed the wire in a large chunk of metal such as Pb-Sn solder. These heavy end connections, and

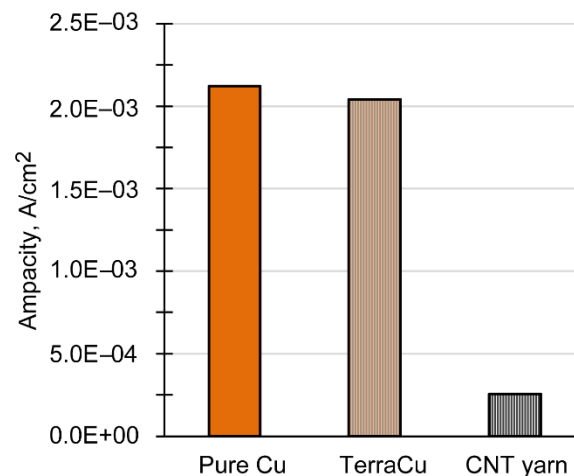


Figure 3.—Ampacity measurement of 20 AWG Pure Cu, Cu-CNT composite TerraCu, and a CNT yarn.

complete encasement enable longitudinal heat flow which corrupts the ampacity measurement. Here is why: It is common for CNT composites to have a texture where in the CNT are primarily arranged longitudinally as a result of the wire drawing process. The thermal conductivity of CNT is not isotropic; the longitudinal thermal conductivity of CNT is very high, but the radial thermal conductivity of CNT is *extremely* low. Ampacity tests that enable or enhance longitudinal heat flow create an advantage for CNT wire that is not usually present in practical applications. The high ampacity results of others may be in part due to the ability of CNT to longitudinally conduct heat. Very good electrical connections were made in the tests presented here, however, these connections were tangential, thus enabled much less surface area for the conduction of heat.

Detailed thermal response of the wires was not a goal of this work. Current and voltage were displayed on the power supply and noted by hand in a log book; time and temperatures were monitored on a computer running data acquisition software and noted by hand in a lab book in real time. However, some of these results are provided for completeness. After slowly and incrementally increasing current to 105 A, the Cu wires took on average 21 min. to fail; the last maximum temperature reading ranged from 734 to 827 °C. The Terracopper samples failed after about 13 min. at a constant current (96.6 A on average); the last maximum temperature reading ranged from 741 to 859 °C. The CNT yarn samples failed after about 10 min at 1 A; the last maximum temperature readings ranged from 237 to 296 °C.

Raman shift

MWNT- Multi-Wall CNT

Figure 4 shows the Raman spectroscopy results normalized to the G-band peak intensity for a single area (A1) on the mixed MWNT BP with the 633 nm laser set at three different powers. The plots fall on top of one another and the D, G, and G'-band peaks are indicated. The characteristic lack of RBM peaks in this MWNT sample confirms the absence of SWNT. The shape of the G-band peak is Lorentzian indicating a characteristically normal amount of semiconductive CNT. The G/D and G/G' ratios are listed in Table I. A G/D ratio near unity indicates a large number of structural defects; a lower ratio (high number of defects) is typically expected for MWNT compared to SWNT due to the multiple graphite layers in MWNT (Ref. 25); however, the MWNT tested appear to have a low number of defects and a G/D ratio about the same as the SWNT.

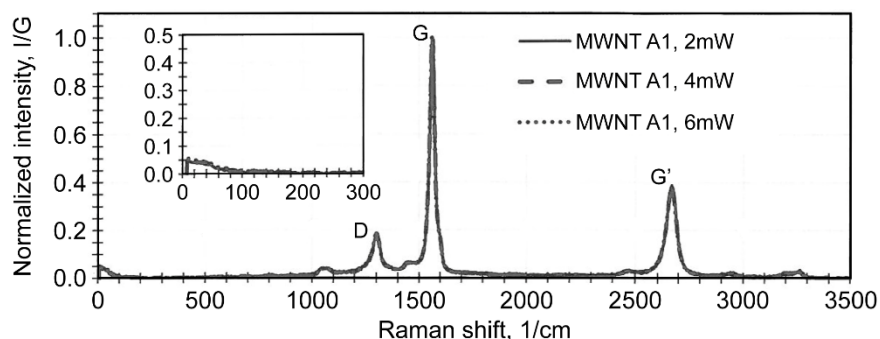


Figure 4.—Raman shift for mixed MWNT Buckypaper using a 633 nm laser.

TABLE I.—RAMAN SHIFT PEAK RATIOS. THE LETTER "A" IN THE SAMPLE DESCRIPTION INDICATES A PARTICULAR AREA; "t" A UNIQUE REPEAT TEST OF A PREVIOUSLY TESTED AREA

Sample and laser power	G/D	G/G'
MWNT A1, 2 mW	5.45	2.586
MWNT A1, 4 mW	5.42	2.632
MWNT A1, 6 mW	5.45	2.639
FWNT 2 mW	16.40	5.00
FWNT A3, 3 mW	16.92	5.52
FWNT A1, 5 mW	16.15	5.12
FWNT A2, 5 mW	15.83	5.58
FWNT 7 mW	14.69	5.37
Mixed SWNT rough 4 mW	7.23	1.564
Mixed SWNT smooth A5, 4 mW	7.02	1.591
Mixed SWNT smooth A6, 4 mW	7.34	1.644
Sorted m-SWNT t0A1, 3 mW	6.13	0.950
Sorted m-SWNT t1A1, 3 mW	6.19	0.945
Sorted m-SWNT t2A1, 3 mW	6.16	0.952
Sorted m-SWNT t3A1, 3 mW	6.12	0.950
Sorted m-SWNT t1A1, 4 mW	6.36	0.962
Sorted m-SWNT A2, 2 mW	6.00	1.005
Sorted m-SWNT A2, 4 mW	6.34	1.050
Sorted m-SWNT A2, 6 mW	6.21	1.028
Sorted m-SWNT rough 4 mW	5.84	1.054
Sorted m-SWNT smooth A3, 4 mW	5.64	1.063
Sorted m-SWNT smooth A4, 4 mW	5.67	1.062

FWNT- Few-Wall CNT, FW100X

Figure 5 shows the Raman results for the FWNT (FW100X, few-walled CNT) powder. The D, G, and G'-band peaks are slightly shifted to the left at the higher laser powers of 5 and 7 mW; and different aspects of the RBM peaks appear to be better resolved at different laser powers. A RBM peak near 261 cm^{-1} is clear when using 2 mW, but this peak is washed out at the higher laser powers; a peak near 247 cm^{-1} can best be seen employing a power of 5 or 7 mW with this peak not seen at 2 mW. Primary RBM peaks are seen at 221 and 158 cm^{-1} and are larger at the lower powers. Weak RBM peaks are present near 198 and 172 cm^{-1} . The double and widened RBM peaks in this FWNT sample are due to the inner and outer tubes of the double and triple-walled tubes that dominate this sample (Ref. 25). The product literature for FW100X states that 83, 11.3 and 5.7 percent of the CNT are either 2, 3, or 4 wall respectively. Equation one is applicable to SWNT thus is not expected to be well suited to this case; but applying it anyway for comparison: the tube diameters corresponding to the primary RBM peaks are 1.12 and 1.57 nm which are not in agreement with SouthWest NanoTechnologies' stated average of 2.45 nm for FW100X. The RBM peak seen near 158 cm^{-1} is expected to be due to s-CNT (Refs. 9 and 12). The shape of the G-band peak is Lorentzian indicating a characteristically normal amount of semi-conductive CNT. This G-band shape, and the split RBM peaks near 70 and 135 cm^{-1} are also present in the FW100X product literature (Ref. 22). The G/D and G/G' ratios are listed in Table I. The G/D ratio for the FWNT tested was higher than any of the other tubes tested and indicates a very low defect density. The G/G' ratio was larger than any of the other tubes tested, which implies a low fraction of metallic CNT.

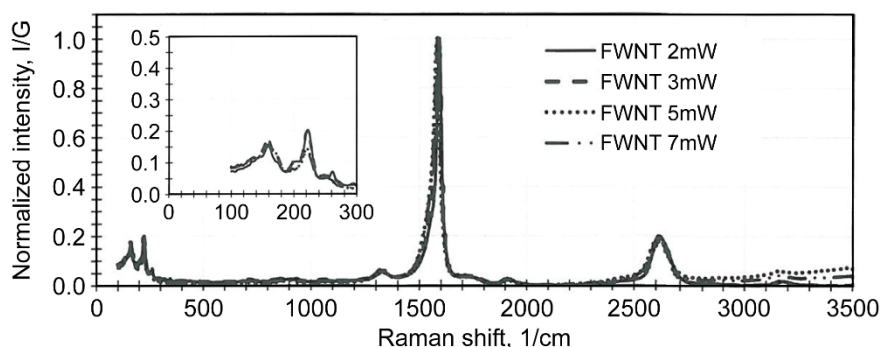


Figure 5.—Raman shift for few wall CNT powder (FWNT) using a 633 nm laser.

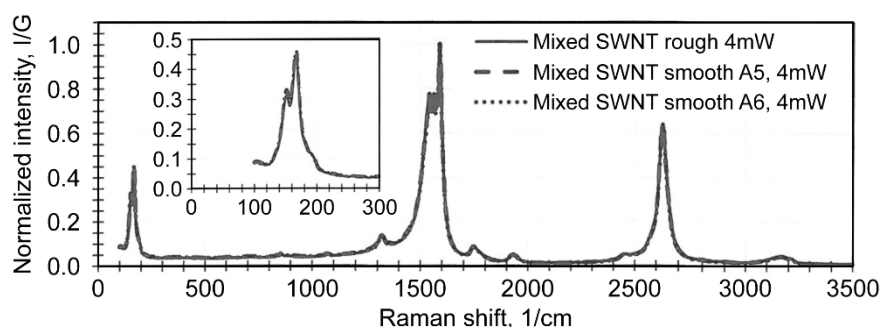


Figure 6.—Raman shift for Buckypapers made for mixed SWNT, Super Pure Tubes, using a 633 nm laser at 4 mW; three different areas tested: the rough side, and No areas on the smooth side A5 and A6; RBM peaks at 151 and 166 1/cm.

Mixed SWNT- Super PureTubes

Figure 6 shows the Raman results for the mixed SWNT. When the BP is made, the “top” side appears to be rougher than the “bottom”. To determine if this had any effect on results areas were examined on both sides of the paper. All results were consistent, falling on top of one another. The primary RBM peaks are at 151 and 166 cm^{-1} , which correspond to approximate diameters of 1.64 and 1.49 nm respectively, which are in good agreement with the diameter range of 1.2 to 1.7 nm in the product literature (Ref. 20). There is also a small RBM peak near 195 cm^{-1} . The very strong RBM peaks near 151 and 166 cm^{-1} appear to be due to s-CNT, and the small peak at 195 cm^{-1} to m-CNT (Refs. 9 and 12). The smooth line shape (compared to Fig. 5) in the RBM range is characteristic of SWNT. The G-band is definitely characteristic of Breit-Wigner-Fano (BWF) line shape however other tests provided by the supplier indicate the sample to be a normal mix of s-CNT and m-CNT. Thus other factors are believed to be responsible for this shape in this case; although a BWF shape can be an indication of metallic tubes, it is not definitive. The shape can also be influenced chiral angle, particularly for SWNT with chiral angles near the zigzag structure, which can be either metallic, or semiconducting (Refs. 5 and 19). The G/D and G/G' ratios are listed in Table I. The G/D indicates low defects and amorphous carbon, though our measurements are not close to the G/D range of 12 to 41 claimed by the manufacturer, though theirs were done using a 513 nm laser. The G/G' ratio was significantly smaller than the ratios for FWNT and MWNT. Results were not affected by the apparent roughness of the top and bottom sides of the paper; for all tests, results were very consistent for a given sample, for all areas and laser powers. The standard deviation of G/G' for the three mixed SWNT areas tested was 3.3 percent.

Sorted SWNT- IsoNanotubes-M

Figure 7 shows nearly all of the Raman results for the BP made from sorted SWNT (IsoNanotubes-M, 95 percent metallic). All data is presented in this way (on the same plot) to see if any significant changes result from varying the laser power, repeat measurements of the same area, or different areas, or different sides of the paper. All data were consistent except for three tests done after an overhaul of the system's computer and a re-alignment of the spectrometer (Ref. 26); one of these tests labeled "Sorted m-SWNT rough 4 mW" is shown as the long dashed red line in Figure 7. The RBM peaks in the pre-overhaul data were at 179 and 194.4 cm^{-1} with a standard deviation of about 2 cm^{-1} . The three post-overhaul tests are presented in Figure 8, and were done to confirm prior tests and determine if the side being tested, the rough top versus the smooth bottom, had any influence on results. There were negligible differences among the three post-overhaul tests; the RBM peaks were at 169 and 185 cm^{-1} , with a standard deviation of less than 1 cm^{-1} . The averages of the RBM peaks for the two sets of data are 174 and 190 cm^{-1} which

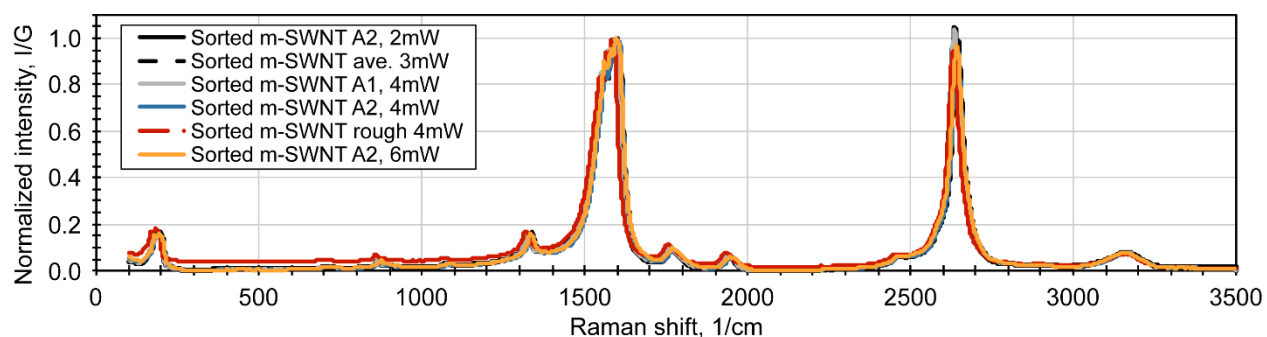


Figure 7.—Raman shift for Buckypapers made from sorted SWNT, IsoNanotubes-M (95 percent metallic) using a 633 nm laser set at various powers; "A" in the legend refers to different areas, "t" to different tests of the same area; the "rough" sample shown by the red long dashed line was done after a system overhaul.

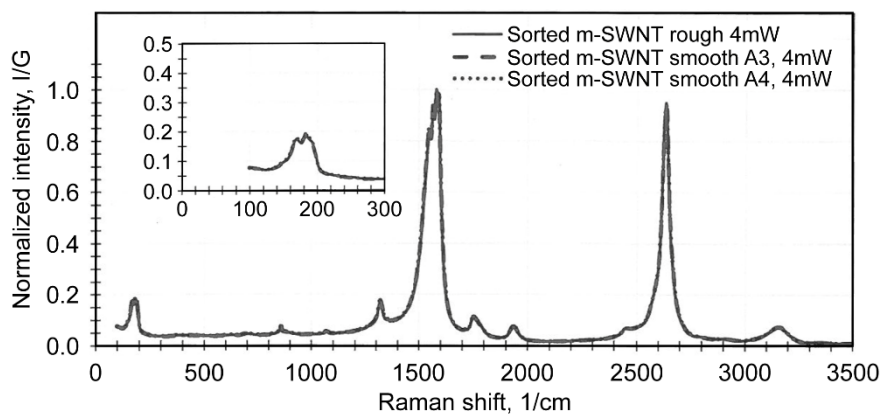


Figure 8.—Raman shift for sorted metallic CNT Buckypaper using a 633 nm laser; These data were taken after computer and spectrometer maintenance; no difference in the data was seen for tests done on different sides of paper.

correspond to SWNT diameters of 1.4 and 1.3 nm respectively, which is in agreement with the stated mean diameter of 1.4 nm for this material (Ref. 20). There is also a noteworthy widening of the 190 cm^{-1} peak which appears to be due to another metallic peak near 197 cm^{-1} . Note that the strong s-CNT RBM peaks near 151 and 166 cm^{-1} in the mixed SWNT (Fig. 6) have completely disappeared, being replaced by the m-CNT peaks near 174 , 190 , and 197 cm^{-1} . The shape of the G-band peak is BWF thus provides an indication of the possibility of metallic tubes. The G/D and G/G' ratios are listed in Table I. The G/D indicates low defects and low amorphous carbon content, though the G/D ratio was not close to the manufacturer's range of 12 to 41 (using a 513 nm laser). The G/G' ratio was significantly smaller than the ratios for MWNT, FWNT, and mixed SWNT.

Results were not affected by the apparent roughness of the top and bottom sides of the paper; results were consistent for all samples regardless of area and laser power. The average G/G' for sorted SWNT was 1.00 with a standard deviation of 0.05.

The G'-band peak was stronger in the sorted SWNT than in the other samples (MWNT, FWNT, and mixed SWNT) which was expected since the sorted SWNT are reported to have a high fraction of metallic tubes (Ref. 19). However, the data show the metallic tube fraction is not the only factor influencing the G'-band peak since the other samples all have very different G/G' ratios yet are expected to have similar m-CNT/s-CNT ratios. The G'-band is a second-order overtone of the D-band and is very sensitive to the stacking order of graphene in multi-wall CNT (Ref. 27). This sensitivity may in part account for G/G' differences among MWNT, FWNT, and SWNT examined. The G/G' ratio may be more effective at quantifying changes in the relative amounts of m-CNT and s-CNT in a given batch of material subjected to a sorting method, rather than among different supplies of CNT with significant variations in diameter and number of walls.

Infrared spectroscopy will be used in future work to provide additional information on relative amounts of m-CNT and s-CNT (Refs. 15 and 20).

Buckypaper Resistivity

Figure 9 shows the electrical resistivity results for the six BP strips measured: three from the Sorted SWNT- IsoNanotubes-M 95 percent metallic paper; and three from the mixed SWNT Super PureTubes (~33 percent metallic) paper. These resistivity measurements are affected by the density and void fraction in the paper. By measuring paper density a more accurate estimate of CNT conductivity was determined.

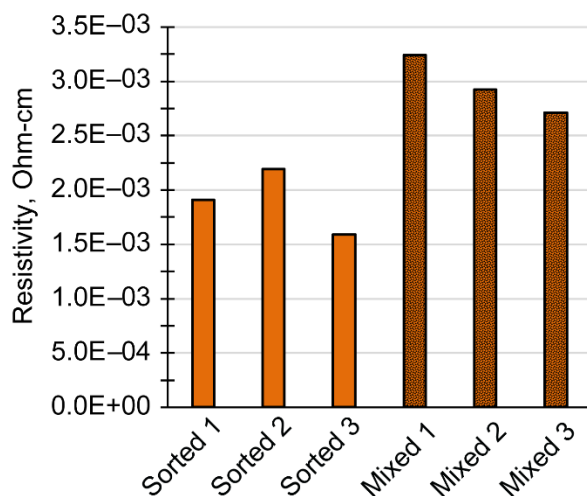


Figure 9.—Resistivity of BP made from sorted SWNT, and mixed SWNT.

Xue found the BP from two vendors to be about 0.01 Ohm-cm, about 4 time higher than Figure 9 values (Ref. 17). Liu et al. reported the measured room temperature resistivity of BP made from MWNT to be 0.02 Ohm-cm, about 10 times higher than the results in this study (Ref. 28). One of the reasons for the high resistivity in Liu's case may be due to the use of MWNT as opposed to SWNT. Multi-wall CNT have a larger diameter, and Yeh has shown the resistivity of BP to increase with tube diameter (Ref. 29). Aldalbahi reported very high BP resistivities in the range of 0.2 Ohm-cm; these high resistivities were likely due to the presence of the biopolymer s-carrageenan in the paper which perhaps wet the tubes and decreased contacts among the tubes, thereby increasing interfacial contact resistance (Ref. 30). On an equal CNT volume percent basis the resistivity of the BP tested in this study had between 10 and 100 times lower resistivity than others found in the literature. The low resistivity of the papers tested is believe to be due to the cleanliness of the CNT; the tubes in IsoNanotubes-M and Super PureTubes have been thoroughly cleaned with efforts made to strip away all functionalized groups used in prior processing steps. This enables good, low resistance contacts among CNT in the BP. These data show the importance of using CNT free of any functional groups or marginally conductive coatings when high conductivity is the goal. This is in agreement with the findings of Xue who observed increases in conductivity with the washing (removing of functional groups) of BP (Ref. 17).

Buckypaper Density

Figure 10 shows the average density of the four samples measured: two each of Sorted SWNT-IsoNanotubes-M 95 percent metallic paper, and mixed SWNT Super PureTubes (~33 percent metallic) paper. These density data enable the determination of void fractions in the different papers using Equations (2) and (3). The volume percent CNT in the BP are shown in Figure 11. The volume fraction of CNT is higher in the mixed SWNT paper. This should give the mixed paper an advantage in conductivity measurements due to more points of contact among tubes; the possibility of this effect will be ignored however in the determination of the effective conductivity of the CNT in the BP. Yang et al. measured the density (and resistivity) of BP made from 20 nm diameter MWNT and found it to be 0.39 g/cm³, with a corresponding resistivity of 0.17 Ohm-cm (Ref. 31). The density Yang et al. achieved was similar to what was observed here (Fig. 10) however their resistivity was much higher; it is believed that this high resistivity was in part due to the relatively large diameter of MWNT used.

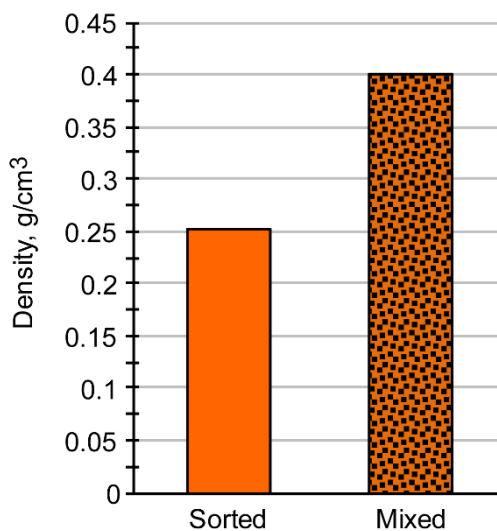


Figure 10.—Density of BP made from sorted SWNT, and mixed SWNT.

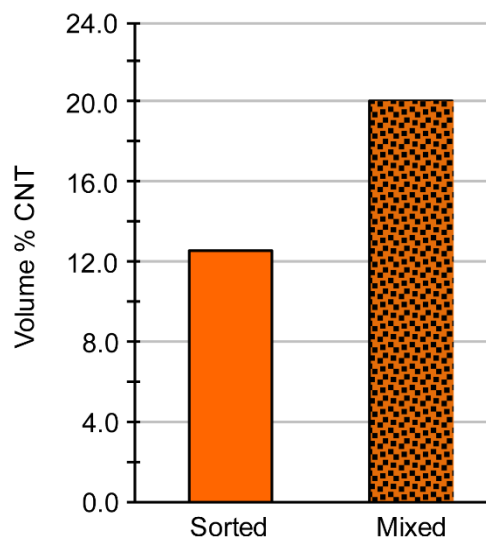


Figure 11.—Carbon nanotube volume percent in sorted SWNT and mixed SWNT Buckypaper.

Conductivity of SWNT in Buckypaper

The average effective conductivity of the CNT in the different SWNT BP (sorted, and mixed) where determined using the following rule-of-mixtures relation:

$$\text{Buckypaper Conductivity} = \sigma_B = 1/\rho_B = \sigma_{\text{CNT}}(\phi_{\text{CNT}}) + \sigma_{\text{void}}(\phi_{\text{void}})$$

where σ_{CNT} is the average, effective conductivity of the CNT in the particular BP, and σ_{void} is the conductivity of the void space in the paper which is set to zero. The resulting conductivities of the tubes in the sorted and mixed SWNT Buckypaper are presented in Figure 12; these data show a 246 percent increase in the CNT conductivity was achieved through sorting and using 95 percent metallic SWNT compared to using mixed (33 percent metallic) SWNT; σ_{CNT} in these cases includes a host of experimental factors affecting conductivity such as interfacial resistances and is not the intrinsic conductivity of the CNT.

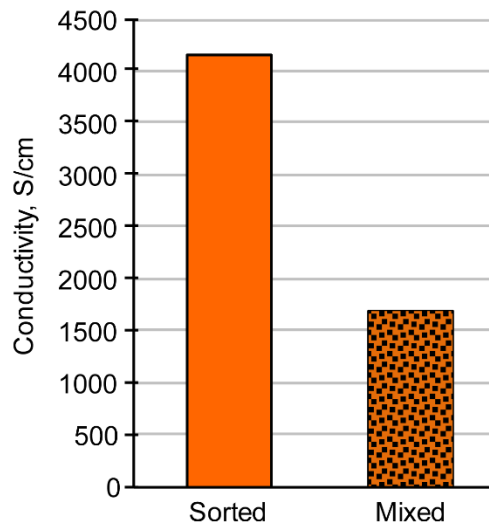


Figure 12.—Average effective conductivity of tubes in sorted and mixed SWNT Buckypaper.

Concluding Remarks

Ampacity: The addition of 5 vol% CNT to high conductivity Cu wire lowered the ampacity of the wire; the decrease is believed to be caused by the low average electrical conductivity of the CNT added to the Cu matrix. The extremely low *thermal* conductivity of CNT in their radial direction is expected to put CNT at a disadvantage compared to materials like Cu because in practical applications heat generated in the wire due to current must be conducted and radiated out radially. Ampacity tests that enable enhanced longitudinal cooling of the wire create a condition that does not represent how the wire will actually be used, and gives an erroneous advantage to CNT.

Raman analysis of BP: Raman spectroscopy can provide indications of metallic CNT, SWNT, FWNT, and MWNT. The locations of m-CNT and s-CNT RBM peaks were in good agreement with literature values, thus provide a tool to detect the presence of specific types of CNT. The G/G' ratios of the different CNT examined in this study varied substantially for samples of similar m-CNT/s-CNT ratios. A quantitative measure of the relative amounts of m-CNT and s-CNT might be possible as long as other variables affecting the spectra are held constant.

Buckypaper Conductivity: The conductivity of the BP tested, both sorted and mixed, were much higher than those found in the literature; this is believed to be due to the use of clean, unfunctionalized SWNT in the BP tested. The conductivity of SWNT BP improved dramatically (+246 percent) with the removal of s-CNT. This implies that the conductivity of CNT conglomerates are dominated by the intrinsic resistance of the CNT rather than contact resistances among tubes, and that conductivity improvements can be achieved through the use of sorted m-CNT rather than mixed CNT.

References

1. H.C. de Groh III, "Consideration of Conductive Motor Winding Materials at Room and Elevated Temperatures," NASA/TM—2015-218882 (2015).
2. A. Rolt, and J. Whurr in *Optimizing Propulsive Efficiency in Aircraft with Boundary Layer Ingesting Distributed Propulsion*, (22nd Int. Symp. on Air Breathing Engines, Phoenix, AZ, 2015), ISABE-2015-20201, pp. 1–10.
3. J.R. Welstead, and J.L. Felder in *Conceptual Design of a Single-Aisle Turboelectric Commercial Transport with Fuselage Boundary Layer Ingestion*, (AIAA SciTech Conf., 54th AIAA Aerospace Sciences Meeting, San Diego, CA, 2016), AIAA-2016-1027, pp. 1–17.
4. M.K. Bradley, and C.K. Droney, "Subsonic Ultra Green Aircraft Research Phase II: N+4 Advanced Concept Development," NASA/CR—2012-217556 (2012).
5. P.R. Bandaru, *J. Nanosci. Nanotechnol.* 7, 3, 1–29 (2007).
6. J. Liu, and M.C. Hersam, *MRS Bull.* 35, 315–321 (2010).
7. K.H. An, J.S. Park, C-M. Yang, S.Y. Jeong, S.C. Lim, C. Kang, J-H. Son, M.S. Jeong, and Y.H. Lee, *J. Am. Chem. Soc.* 127, 5196–5203 (2005).
8. G. Zhang, P. Qi, X. Wang, Y. Lu, X. Li, R. Tu, S. Bangsaruntip, D. Mann, L. Zhang, and H. Dai, *Science* 314, 974–977 (2006).
9. L. Ding, A. Tselev, J. Wang, D. Yuan, H. Chu, T.P. McNicholas, Y. Li, and J. Liu, *Nano Lett.* 9, 2, 800–805 (2009).
10. L. Qu, F. Du, and L. Dai, *Nano Lett.* 8, 2682 (2008).
11. G. Hong, B. Zhang, B. Peng, J. Zhang, W.M. Choi, J-Y. Choi, J.M. Kim, and Z. Liu, *J. Am. Chem. Soc.* 131, 41, 14642–14643 (2009).
12. A.R. Harutyunyan, G. Chen, T.M. Paronyan, E.M. Pigos, O.A. Kuznetsov, K. Hewaparakrama, S.M. Kim, D. Zakharov, E.A. Stach, and G.U. Sumanasekera, *Science* 326, 116–120, (2009).
13. R. Krupke, F. Hennrich, H. v. Lohneysen, M.M. Kappes, *Science*, 301, 344–347 (2003).
14. M.C. LeMieux, M. Roberts, S. Barman, Y.W. Jin, J.M. Kim, and Z. Bao, *Science* 321, 101–104 (2008).

15. M.S. Arnold, A.A. Green, J.F. Hulvat, S.I. Stupp, and M.C. Hersam, *Nat. Nanotechnol.* 1, 60–65 (2006).
16. I. Yahya, F. Bonaccorso, S.K. Clowes, A.C. Ferrari, and S.R. P. Silva, *Carbon* 93, 574–594 (2015).
17. Y. Xue, “Experimental Study of Electrical Conductivity of Carbon Nanotube, Nanofiber Buckypapers and Their Composites,” Master’s Thesis, Florida State University, Tallahassee, FL (2007).
18. M.S. Dresselhaus, G. Dresselhaus, R. Saito, and A. Jorio, *Phys. Rep.* 409, 47–99 (2005).
19. K.K. Kim, J.S. Park, S.J. Kim, H.Z. Geng, K.H. An, C-M. Yang, K. Sato, R. Saito, and Y.H. Lee, *Phys. Rev. B* 76, 205426 (2007).
20. NanoIntegris Technical Data Sheet, IsoNanotubes-M, -S, and PureTubes, (NanoIntegris, Skokie, IL, 2015). <http://raymor.com/wp-content/uploads/2015/01/Carbon-Nanotubes-Technical-Data-Sheet.pdf> (last retrieved Jan. 19, 2016).
21. L.A. Aroian, et al. *Van Nostrand’s Scientific Encyclopedia, Fourth Edition* (Van Nostrand Co., Inc., 1968) p. 1632.
22. SouthWest NanoTechnologies, Technical Data Sheet, FW100X, Few-Wall Carbon Nanotubes, 4.15.2015 Rev 5 (2015). http://www.swentnano.com/uploads/3/0/7/0/30708225/fw100x_tds_rev5.pdf (last retrieved Jan. 19, 2016).
23. C. Subramaniam, T. Yamada, K. Kobashi, A. Sekiguchi, D. N. Futaba, M. Yamura, and K. Heta, *Nat. Commun.* 4, 2202 (2013).
24. C. Dyke, L.M. Jacob, D. Madden, and V. Barrera in *Ultrahigh Conductivity Umbilicals: Polymer Nanotube Umbilicals* (Offshore Technology Conference, Houston, TX, 2013), OTC-24255, pp. 1–5.
25. S. Costa, E. Borowiak-Palen, M. Kruszynska, A. Bachmatiuk, and R. J. Kalenczuk, *Mater. Sci.-Poland* 26, 2, 433–440 (2008).
26. P. Henson, “Optical Alignment for High Performance Dispersive Raman Microscopy,” Technical Note: 51723 (Thermo Fisher Scientific, Madison WI, 2008).
27. M.A. Pimenta, G. Dresselhaus, M.S. Dresselhaus, L.G. Cancado, A. Jorio, and R. Saito, *Phys. Chem. Chem. Phys.* 9, 1276–1291 (2007).
28. J-H. Liu, H-Y. Miao, S. Lakshmanan, L-C. Wang, and R-H. Tsai, *J. Nanomater.* 2013 (2013). <http://www.hindawi.com/journals/jnm/2013/635647/> (last retrieved Feb. 3, 2016).
29. C-S. Yeh, “A Study of Nanostructure and Properties of Mixed Nanotube Buckypaper Materials: Fabrication, Process Modeling Characterization, and Property Modeling,” Ph.D. Thesis, Florida State University, Tallahassee, FL (2007), p. 147.
30. A. Aldalbahi, *Carbon*, 50, 3, 1197–1208 (2012).
31. K. Yang, J. He, P. Puneet, Z. Su, M.J. Skovel, J. Gaillard, T.M. Tritt, and A.M. Rao, *J. Phys. Condens. Matter* 22, 1–6 (2010). <http://iopscience.iop.org/article/10.1088/0953-8984/22/33/334215/meta;jsessionid=5825D471AA4D0BAE435C931F8FBABC21.c2.iopscience.cld.iop.org> (last retrieved Feb 2, 2016).

